Super and subcritical nonlinear nonlocal analysis of NSGT nanotubes conveying nanofluid

Ali Farajpour[1] · Mergen H. Ghayesh[1] · Hamed Farokhi[2]

Abstract

An advanced nonlinear continuum model is presented to analyse the super and subcritical nonlinear behaviour of nanotubes. The nanoscale system is used to convey fluid flow at nanoscale levels. Due to the restrictions of one-parameter size-dependent models, a more comprehensive nonlinear coupled model containing two different size parameters is introduced using the nonlocal strain gradient theory (NSGT). Both axial and transverse inertial terms are taken into consideration, leading to more accurate results for nanotubes conveying fluid. In addition, since the mean free path of molecules is not negligible compared to the diameter of the tube at nanoscales, the Beskok–Karniadakis approach is implemented. The NSGT, Galerkin's technique and continuation method are finally employed to derive, discretise and solve the coupled nonlinear equations, respectively. The frequency–amplitude response, modal interactions and the possibility of energy transfer between modes are examined in both supercritical and subcritical flow regimes.

1 Introduction

In recent years, various nanotubes have been synthesised and used in nanoscale electromechanical systems. The widespread application of nanotubes is due to their excellent mechanical, thermal and electrical properties. For instance, carbon nanotubes have an exceptional strength and a high thermal conductivity, leading to the extensive applications of them in different nanosystems such as nanoresonators, nanogenerators, thermal conductors and scaffolds for bone growth (De Volder et al. 2013). Strong nonlinear dynamics has been found in the fundamental structures of many microelectromechanical and nanoelectromechanical systems (MEMS and NEMS) (Farokhi and Ghayesh 2016, 2018; Ghayesh and Farokhi 2018; Sassi and Najar 2018), making the investigation of this phenomenon

extremely important in analysing MEMS and NEMS devices.

The vibration response of macroscale structures has widely been explored via the classical elasticity (Ghayesh et al. 2013a; Ghayesh and Moradian 2011; Malekzadeh 2007; Malekzadeh and Vosoughi 2009). However, since classical continuum-based models lead to size-independent results for small-scale structures, they are modified to include size effects (Babaei and Yang 2019; Ebrahimi and Barati 2019; Farajpour et al. 2018b; Farajpour et al. 2018c; Ghayesh and Farajpour 2018b; Lin et al. 2018; Sahmani and Aghdam 2018), and accurately estimate the mechanical behaviour at small-scales (Farokhi et al. 2018a, 2018b; Ghayesh 2018a, 2019; Kamali et al. 2018; Pradiptya and Ouakad 2018; Yayli 2018). Various modified continuum-based models involving the nonlocal (Farajpour et al. 2017; Reddy 2010), couple stress (Ghayesh et al. 2016a; Nejad et al. 2017) and a theory incorporating the gradient of strain (Akgöz and Civalek 2011; Ghayesh et al. 2013b) have been developed and utilised for small-scale structures (Farokhi and Ghayesh 2015; Ghayesh et al. 2016b; Farajpour et al. 2018d; Gholipour et al. 2015; Farajpour et al. 2019b). Recently, an advanced version of the nonlocal theory, which includes strain gradient effects, has attracted much attention in the continuum modelling of nanostructures (Lim et al. 2015; Zhu and Li 2017). This size-dependent theory is technically termed as "nonlocal strain gradient".

✉ Ali Farajpour
ali.farajpourouderji@adelaide.edu.au

Mergen H. Ghayesh
mergen.ghayesh@adelaide.edu.au

Hamed Farokhi
hamed.farokhi@northumbria.ac.uk

1 School of Mechanical Engineering, University of Adelaide, Adelaide, SA 5005, Australia

2 Department of Mechanical and Construction Engineering, Northumbria University, Newcastle upon Tyne NE1 8ST, UK

In this work, using this theory, size effects on the mechanical response are captured.

Modified continuum-based models have widely been presented for the vibration, bending and instability analyses of nanotubes. In one pioneering study, Zhang et al. (2005) presented a nonlocal model to analyse the free vibration of a system of two nanotubes. In another work, Reddy and Pang (2008) presented different scale-dependent beam models for the mechanical behaviours of nanotubes involving the static deformation, oscillation and stability responses; they utilised the nonlocal constitutive relation for developing the scale-dependent formulation. Malekzadeh and Shojaee (2013b) developed a nonlinear beam model with incorporation of both nonlocal and surface influences for analysing the large-amplitude oscillations of nanobeams; they presented numerical results based on both Euler–Bernoulli and Timoshenko theories of beams. Moreover, Malekzadeh and Shojaee (2013a) analysed the static stability of quadrilateral laminated sheets made of several layers reinforced with carbon nanotubes; they used a first-order theory of shear deformations to model the quadrilateral laminated sheet. Khaniki et al. (2018) also developed a two-phase scale-dependent model for dynamics of nanoscale beams; the nanosystem was embedded in a varying elastic medium. Aydogdu and Filiz (2011) proposed a scale-dependent model for mass nanosensors using nanotubes; the axial vibration of carbon nanotubes was exploited for mass detection at nanoscales. In addition, Aydogdu (2014) employed the nonlocal elasticity for analysing axial wave propagations in multi-walled nanotubes; the effects of van der Waals forces between various walls on the wave propagation were captured via an analytical model. In another study, Malekzadeh et al. (2014) investigated the free vibration of a skew small-scale plate with large displacements capturing size effects; surface effects were also taken into consideration in the model. Setoodeh and Afrahim (2014) utilised the strain gradient theory to explore the large-amplitude dynamics of microscale pipes conveying fluid; in the formulation, it was assumed that the pipe was made of functionally graded materials. More recently, Li et al. (2016) analysed the wave dispersion in nanotubes with viscoelastic properties via a nonlocal strain gradient theory (NSGT).

In addition to pure nanotube systems, the mechanics of fluid-conveying nanotubes has attracted noticeable attention in the literature (Dai et al. 2015; Wang et al. 2010). Understanding the mechanical behaviour of these systems is important in applications such as drug delivery systems and microfluidics-based devices. Although some valuable research works have been performed on the fluid-conveying nanotubes (Ansari et al. 2016; Maraghi et al. 2013; Soltani et al. 2010; Zeighampour and Beni 2014), further investigation is required to understand the large-

amplitude dynamics of nanotubes conveying nanofluid since the majority of previously published works are restricted to small deformations. In addition, for the sake of simplification, only transverse motion has been analysed. Furthermore, to the best of our knowledge, modal interactions and energy transfer between different modes of fluid-conveying nanotubes have not been examined yet. In the present paper, an advanced scale-dependent model is presented for the frequency response of a nanotube with large amplitudes of vibrations. The elastic nanotube is used to convey fluid flow. The Beskok–Karniadakis approach is implemented to consider slip boundary conditions on the nonlinear behaviour. The NSGT, Galerkin's approach and continuation scheme are, respectively, utilised to derive, discretise and solve the motion equations. The frequency–amplitude plots are constructed for studying the possibility of energy transfer between modes together with modal interaction in both supercritical and subcritical regimes.

2 A NSGT-based model

To develop a continuum model, a single nanotube of a high length-to-thickness ratio is taken into account as shown in Fig. 1. The nanotube is used to convey fluid flow at nanoscales. It is assumed that the tube is perfectly straight. In addition, there is no internal friction in both the fluid and solid parts. The length, mass per length and diameter of the nanotube are, respectively, indicated by L, m and d_o. Furthermore, M is utilised to indicate the mass per length of the nanofluid. For the displacement components of the tube, we assume that $(u, w) =$ (axial displacement, transverse displacement). It is assumed that the effects of shear deformation are negligible. In addition, the tube cross-section is constant in this analysis. Only geometrical nonlinearity caused by the stretching influence of the tube centreline is captured. Using Euler–Bernoulli theory and incorporating the geometrical nonlinearity, the strain is
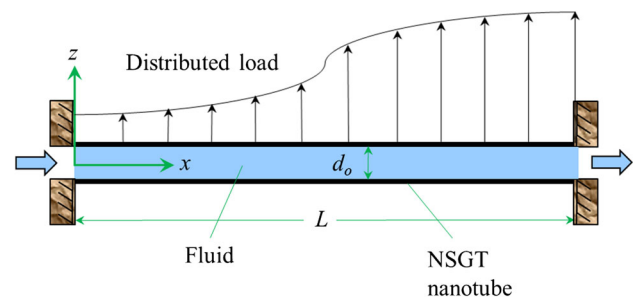

Fig. 1 A NSGT nanotube conveying fluid subject to a distributed load

$$\varepsilon_{xx} = \frac{\partial u}{\partial x} + \frac{1}{2}\left(\frac{\partial w}{\partial x}\right)^2 - z\left(\frac{\partial^2 w}{\partial x^2}\right). \tag{1}$$

In reality, taking into account the effects of nonlinearity is important to develop precise modelling (Ghayesh and Farokhi 2015a; Gholipour et al. 2018a, b; Farajpour et al. 2018e; Ghayesh et al. 2019).

The force and couple resultants related to the total stress ($\sigma_{xx}^{(tot)}$) are as

$$N_{xx} = \int_A \sigma_{xx}^{(tot)} dA, \quad M_{xx} = \int_A z\sigma_{xx}^{(tot)} dA. \tag{2}$$

Using the NSGT, one can express the total stress in terms of the strain as.

$$\sigma_{xx}^{(tot)} - (e_0 a)^2 \nabla^2 \sigma_{xx}^{(tot)} = E\left(1 - l_{sg}^2 \nabla^2\right)\left[\frac{\partial u}{\partial x} + \frac{1}{2}\left(\frac{\partial w}{\partial x}\right)^2\right] - zE\left(1 - l_{sg}^2 \nabla^2\right)\left(\frac{\partial^2 w}{\partial x^2}\right), \tag{3}$$

in which ∇^2, l_{sg}, E, e_0 and a are the Laplacian operator, strain gradient parameter, elasticity constant, calibration coefficient and internal characteristic size, respectively (Farajpour et al. 2018a; Ghayesh and Farajpour 2018a, 2019). In view of the above constitutive equation (i.e. Eq. (3)), the following relations are obtained from Eq. (2)

$$N_{xx} = EA\left[\frac{1}{2}\left(\frac{\partial w}{\partial x}\right)^2 + \frac{\partial u}{\partial x}\right] - EAl_{sg}^2 \nabla^2\left[\frac{1}{2}\left(\frac{\partial w}{\partial x}\right)^2 + \frac{\partial u}{\partial x}\right] + (e_0 a)^2 \nabla^2 N_{xx}, \tag{4}$$

$$M_{xx} = -EI\frac{\partial^2 w}{\partial x^2} + EIl_{sg}^2 \nabla^2 \frac{\partial^2 w}{\partial x^2} + (e_0 a)^2 \nabla^2 M_{xx}, \tag{5}$$

where I denotes the second moment area. Let us indicate the classical and higher-order stresses by σ_{xx} and $\sigma_{xx}^{(1)}$, respectively (Farajpour et al. 2019a; Lim et al. 2015). For the strain energy (Π_s), one can write

$$\delta\Pi_s = \int_0^L \int_A \left(\sigma_{xx}\delta\varepsilon_{xx} + \sigma_{xx}^{(1)}\frac{\partial}{\partial x}\delta\varepsilon_{xx}\right) dA dx$$
$$= \left[\int_A \sigma_{xx}^{(1)}\delta\varepsilon_{xx} dA\right]_0^L + \int_0^L \int_A \sigma_{xx}^{(tot)}\delta\varepsilon_{xx} dA dx, \tag{6}$$

where

$$\sigma_{xx}^{(tot)} = \sigma_{xx} - \frac{\partial\sigma_{xx}^{(1)}}{\partial x}, \tag{7}$$

Assuming U is the fluid velocity, the kinetic energy of the nanosystem (T_k) is (Ghayesh et al. 2018; Paidoussis 1998)

$$T_k = \frac{1}{2}\int_0^L m\left(\frac{\partial w}{\partial t}\right)^2 dx + \frac{1}{2}\int_0^L m\left(\frac{\partial u}{\partial t}\right)^2 dx$$
$$+ \frac{1}{2}\int_0^L M\left[\frac{\partial u}{\partial t} + \kappa_v U\left(1 + \frac{\partial u}{\partial x}\right)\right]^2 dx \tag{8}$$
$$+ \frac{1}{2}\int_0^L M\left(\frac{\partial w}{\partial t} + \kappa_v U\frac{\partial w}{\partial x}\right)^2 dx.$$

Here a correction factor for the fluid velocity (κ_v) is utilised for capturing slip conditions at the wall. Using the Beskok–Karniadakis approach (Beskok and Karniadakis 1999), one obtains

$$\kappa_v = (\lambda Kn + 1)\left[\left(\frac{4Kn}{Kn + 1}\right)\left(\frac{2 - \sigma_v}{\sigma_v}\right) + 1\right], \tag{9}$$

where

$$\lambda = \frac{2\lambda_0}{\pi}\tan^{-1}[\alpha_0 (Kn)^{\alpha_1}], \tag{10}$$

in which Kn is the Knudsen number. For nanotubes, it is commonly assumed that $\sigma_v = 0.7$, $\alpha_0 = 4$, $\alpha_1 = 0.4$ and $\lambda_0 = 64/15\pi$. Assuming the amplitude $F(x)$ and frequency ω for the applied load, the external work is given by

$$\delta W_q = \int_0^L q\delta w \, dx. \tag{11}$$

where

$$q = F(x)\cos(\omega t). \tag{12}$$

For deriving the motion equations, Hamilton's principle is employed as follows

$$\int_{t_1}^{t_2} \left(\delta W_q + \delta T_k - \delta\Pi_s\right) dt = 0. \tag{13}$$

Substituting Eqs. (6), (8) and (11) into the above principle, one can obtain

$$\frac{\partial N_{xx}}{\partial x} - \left((m + M)\frac{\partial^2 u}{\partial t^2} + 2M\kappa_v U\frac{\partial^2 u}{\partial t\partial x} + M\kappa_v^2 U^2\frac{\partial^2 u}{\partial x^2}\right) = 0, \tag{14}$$

$$\frac{\partial^2 M_{xx}}{\partial x^2} + \frac{\partial}{\partial x}\left(N_{xx}\frac{\partial w}{\partial x}\right) + F(x)\cos(\omega t)$$
$$- \left((m + M)\frac{\partial^2 w}{\partial t^2} + 2M\kappa_v U\frac{\partial^2 w}{\partial t\partial x} + M\kappa_v^2 U^2\frac{\partial^2 w}{\partial x^2}\right)$$
$$= 0. \tag{15}$$

Using the above equations (i.e. Eqs. (14) and (15)) together with Eqs. (4) and (5), the motion equations are derived as

$$EA\left(\frac{\partial^2 u}{\partial x^2}+\frac{\partial w}{\partial x}\frac{\partial^2 w}{\partial x^2}\right)-EAl_{sg}^2\nabla^2\left(\frac{\partial^2 u}{\partial x^2}+\frac{\partial w}{\partial x}\frac{\partial^2 w}{\partial x^2}\right)$$

$$=(m+M)\frac{\partial^2 u}{\partial t^2}+2M\kappa_v U\frac{\partial^2 u}{\partial t\partial x}+M\kappa_v^2 U^2\frac{\partial^2 u}{\partial x^2}$$

$$-(e_0 a)^2\nabla^2\left[(m+M)\frac{\partial^2 u}{\partial t^2}+2M\kappa_v U\frac{\partial^2 u}{\partial t\partial x}+M\kappa_v^2 U^2\frac{\partial^2 u}{\partial x^2}\right],$$

(16)

$$-EI\frac{\partial^4 w}{\partial x^4}+EIl_{sg}^2\nabla^2\frac{\partial^4 w}{\partial x^4}+F(x)\cos(\omega t)-(e_0 a)^2\cos(\omega t)\nabla^2 F(x)$$

$$+EA\frac{\partial^2 w}{\partial x^2}\left[\frac{\partial u}{\partial x}+\frac{1}{2}\left(\frac{\partial w}{\partial x}\right)^2\right]+EA\frac{\partial w}{\partial x}\left(\frac{\partial^2 u}{\partial x^2}+\frac{\partial w}{\partial x}\frac{\partial^2 w}{\partial x^2}\right)$$

$$-l_{sg}^2 EA\frac{\partial^2 w}{\partial x^2}\nabla^2\left[\frac{\partial u}{\partial x}+\frac{1}{2}\left(\frac{\partial w}{\partial x}\right)^2\right]-l_{sg}^2 EA\frac{\partial w}{\partial x}\nabla^2\left(\frac{\partial^2 u}{\partial x^2}+\frac{\partial w}{\partial x}\frac{\partial^2 w}{\partial x^2}\right)$$

$$+(e_0 a)^2\frac{\partial^2 w}{\partial x^2}\left[(m+M)\frac{\partial^3 u}{\partial x\partial t^2}+2M\kappa_v U\frac{\partial^3 u}{\partial t\partial x^2}+M\kappa_v^2 U^2\frac{\partial^3 u}{\partial x^3}\right]$$

$$+(e_0 a)^2\frac{\partial w}{\partial x}\left[(m+M)\frac{\partial^4 u}{\partial x^2\partial t^2}+2M\kappa_v U\frac{\partial^4 u}{\partial t\partial x^3}+M\kappa_v^2 U^2\frac{\partial^4 u}{\partial x^4}\right]$$

$$-(e_0 a)^2\nabla^2\left\{EA\frac{\partial^2 w}{\partial x^2}\left[\frac{\partial u}{\partial x}+\frac{1}{2}\left(\frac{\partial w}{\partial x}\right)^2\right]+EA\frac{\partial w}{\partial x}\left(\frac{\partial^2 u}{\partial x^2}+\frac{\partial w}{\partial x}\frac{\partial^2 w}{\partial x^2}\right)\right.$$

$$-l_{sg}^2 EA\frac{\partial^2 w}{\partial x^2}\nabla^2\left[\frac{\partial u}{\partial x}+\frac{1}{2}\left(\frac{\partial w}{\partial x}\right)^2\right]-l_{sg}^2 EA\frac{\partial w}{\partial x}\nabla^2\left(\frac{\partial^2 u}{\partial x^2}+\frac{\partial w}{\partial x}\frac{\partial^2 w}{\partial x^2}\right)$$

$$+(e_0 a)^2\frac{\partial^2 w}{\partial x^2}\left[(m+M)\frac{\partial^3 u}{\partial x\partial t^2}+2M\kappa_v U\frac{\partial^3 u}{\partial t\partial x^2}+M\kappa_v^2 U^2\frac{\partial^3 u}{\partial x^3}\right]$$

$$\left.+(e_0 a)^2\frac{\partial w}{\partial x}\left[(m+M)\frac{\partial^4 u}{\partial x^2\partial t^2}+2M\kappa_v U\frac{\partial^4 u}{\partial t\partial x^3}+M\kappa_v^2 U^2\frac{\partial^4 u}{\partial x^4}\right]\right\}$$

$$=(m+M)\frac{\partial^2 w}{\partial t^2}+2M\kappa_v U\frac{\partial^2 w}{\partial t\partial x}+M\kappa_v^2 U^2\frac{\partial^2 w}{\partial x^2}$$

$$-(e_0 a)^2\nabla^2\left[(m+M)\frac{\partial^2 w}{\partial t^2}+2M\kappa_v U\frac{\partial^2 w}{\partial t\partial x}+M\kappa_v^2 U^2\frac{\partial^2 w}{\partial x^2}\right].$$

(17)

Now without losing the generality, a set of dimensionless parameters is utilised as follows

$$u^*=\frac{u}{d_o},\ w^*=\frac{w}{d_o},\ x^*=\frac{x}{L},\ \chi_{sg}=\frac{l_{sg}}{L},$$

$$\Xi=\frac{AL^2}{I},\ \chi_{nl}=\frac{e_0 a}{L},\ s=\frac{L}{d_o},\ \bar{M}=\frac{M}{M+m},$$

$$\omega^*=\sqrt{\frac{L^4(m+M)}{EI}}\omega,\ t^*=\frac{t}{L^2}\sqrt{\frac{EI}{m+M}},$$

$$U^*=\sqrt{\frac{M}{EI}}UL,\ F^*=\frac{FL^4}{EId_o},\ \nabla^2=\frac{\partial^2}{\partial x^{*2}},$$

(18)

Here ∇^2 denotes the dimensionless Laplacian operator. Employing Eq. (18) together with Eqs. (16) and (17), the dimensionless motion equations are derived as
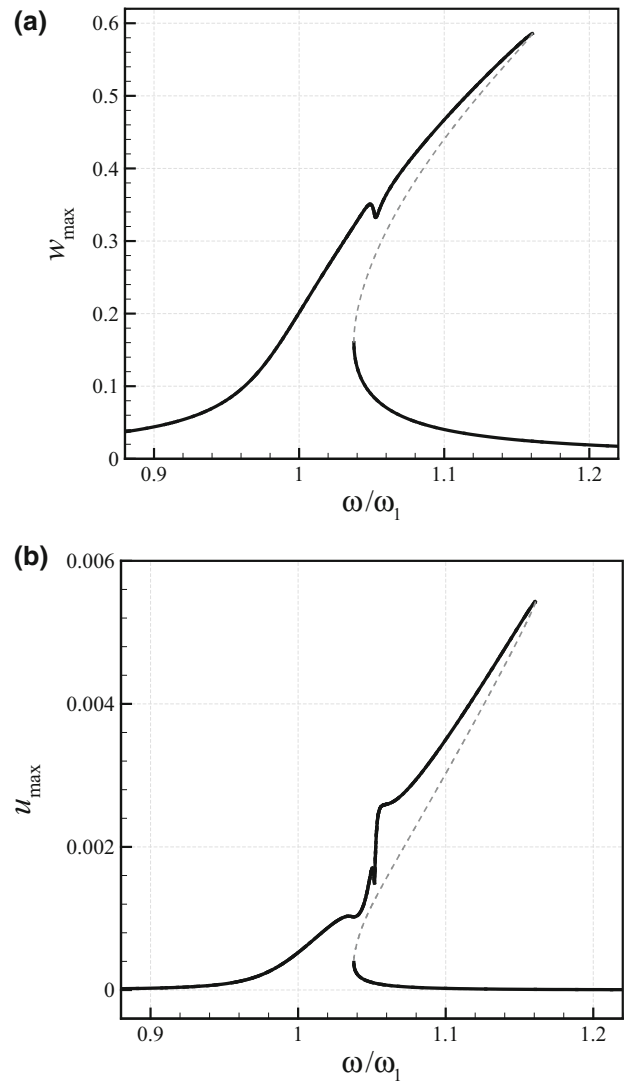
Fig. 2 Change of maximum transverse and axial displacements versus the frequency ratio in the subcritical flow regime for $F_1=2.0$ and $U=3.25$; **a** w_{max} at $x=0.5$; **b** u_{max} at $x=0.657$; $\omega_1=15.5031$

$$\frac{\partial^2 u}{\partial t^2}+2\kappa_v\sqrt{\bar{M}}U\frac{\partial^2 u}{\partial t\partial x}+\kappa_v^2 U^2\frac{\partial^2 u}{\partial x^2}$$

$$-\chi_{nl}^2\left(\frac{\partial^4 u}{\partial x^2\partial t^2}+2\kappa_v\sqrt{\bar{M}}U\frac{\partial^4 u}{\partial t\partial x^3}+\kappa_v^2 U^2\frac{\partial^4 u}{\partial x^4}\right)$$

$$-\Xi\left(\frac{\partial^2 u}{\partial x^2}+\frac{1}{s}\frac{\partial w}{\partial x}\frac{\partial^2 w}{\partial x^2}\right)+\Xi\chi_{sg}^2\left(\frac{\partial^4 u}{\partial x^4}+\frac{3}{s}\frac{\partial^2 w}{\partial x^2}\frac{\partial^3 w}{\partial x^3}+\frac{1}{s}\frac{\partial w}{\partial x}\frac{\partial^4 w}{\partial x^4}\right)=0,$$
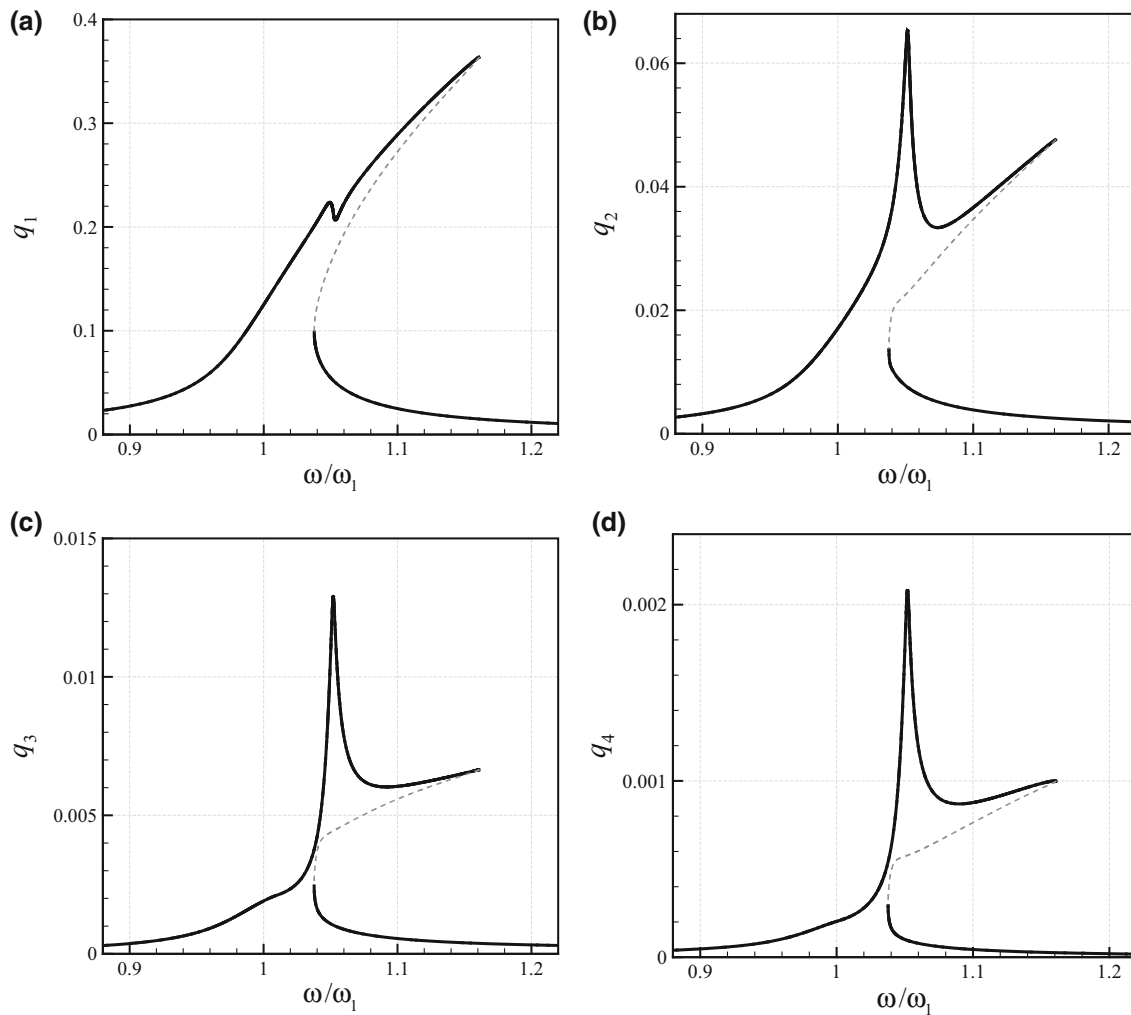
(19)

Fig. 3 Change of **a** q_1, **b** q_2, **c** q_3 and **d** q_4 versus the ratio of the excitation frequency to the natural one in the subcritical flow regime

$$\frac{\partial^2 w}{\partial t^2} + 2\kappa_v\sqrt{\bar{M}}U\frac{\partial^2 w}{\partial t\partial x} + \kappa_v^2 U^2\frac{\partial^2 w}{\partial x^2}$$
$$- \chi_{nl}^2\left(\frac{\partial^4 w}{\partial x^2\partial t^2} + 2\kappa_v\sqrt{\bar{M}}U\frac{\partial^4 w}{\partial t\partial x^3} + \kappa_v^2 U^2\frac{\partial^4 w}{\partial x^4}\right)$$
$$+ \frac{\partial^4 w}{\partial x^4} - \chi_{sg}^2\frac{\partial^6 w}{\partial x^6} - F_1\cos(\omega t) - \frac{\Xi}{s^2}\left\{\frac{\partial^2 w}{\partial x^2}\left[s\frac{\partial u}{\partial x} + \frac{1}{2}\left(\frac{\partial w}{\partial x}\right)^2\right]\right.$$
$$+ \frac{\partial w}{\partial x}\left(s\frac{\partial^2 u}{\partial x^2} + \frac{\partial w}{\partial x}\frac{\partial^2 w}{\partial x^2}\right) - \chi_{sg}^2\frac{\partial^2 w}{\partial x^2}\left[s\frac{\partial^3 u}{\partial x^3} + \left(\frac{\partial^2 w}{\partial x^2}\right)^2 + \frac{\partial w}{\partial x}\frac{\partial^3 w}{\partial x^3}\right]$$
$$- \chi_{sg}^2\frac{\partial w}{\partial x}\left[s\frac{\partial^4 u}{\partial x^4} + 3\frac{\partial^2 w}{\partial x^2}\frac{\partial^3 w}{\partial x^3} + \frac{\partial w}{\partial x}\frac{\partial^4 w}{\partial x^4}\right]$$

$$+ \frac{s}{\Xi}\chi_{nl}^2\frac{\partial^2 w}{\partial x^2}\left[\frac{\partial^3 u}{\partial x\partial t^2} + 2\kappa_v\sqrt{\bar{M}}U\frac{\partial^3 u}{\partial t\partial x^2} + \kappa_v^2 U^2\frac{\partial^3 u}{\partial x^3}\right]$$
$$\left.+ \frac{s}{\Xi}\chi_{nl}^2\frac{\partial w}{\partial x}\left[\frac{\partial^4 u}{\partial x^2\partial t^2} + 2\kappa_v\sqrt{\bar{M}}U\frac{\partial^4 u}{\partial t\partial x^3} + \kappa_v^2 U^2\frac{\partial^4 u}{\partial x^4}\right]\right\}$$
$$+ \frac{\Xi}{s^2}\chi_{nl}^2\frac{\partial^2}{\partial x^2}\left\{\frac{\partial^2 w}{\partial x^2}\left[s\frac{\partial u}{\partial x} + \frac{1}{2}\left(\frac{\partial w}{\partial x}\right)^2\right] + \frac{\partial w}{\partial x}\left(s\frac{\partial^2 u}{\partial x^2} + \frac{\partial w}{\partial x}\frac{\partial^2 w}{\partial x^2}\right)\right.$$
$$- \chi_{sg}^2\frac{\partial^2 w}{\partial x^2}\left[s\frac{\partial^3 u}{\partial x^3} + \left(\frac{\partial^2 w}{\partial x^2}\right)^2 + \frac{\partial w}{\partial x}\frac{\partial^3 w}{\partial x^3}\right]$$
$$- \chi_{sg}^2\frac{\partial w}{\partial x}\left(s\frac{\partial^4 u}{\partial x^4} + 3\frac{\partial^2 w}{\partial x^2}\frac{\partial^3 w}{\partial x^3} + \frac{\partial w}{\partial x}\frac{\partial^4 w}{\partial x^4}\right)$$
$$+ \frac{s}{\Xi}\chi_{nl}^2\frac{\partial^2 w}{\partial x^2}\left[\frac{\partial^3 u}{\partial x\partial t^2} + 2\kappa_v\sqrt{\bar{M}}U\frac{\partial^3 u}{\partial t\partial x^2} + \kappa_v^2 U^2\frac{\partial^3 u}{\partial x^3}\right]$$
$$\left.+ \frac{s}{\Xi}\chi_{nl}^2\frac{\partial w}{\partial x}\left[\frac{\partial^4 u}{\partial x^2\partial t^2} + 2\kappa_v\sqrt{\bar{M}}U\frac{\partial^4 u}{\partial t\partial x^3} + \kappa_v^2 U^2\frac{\partial^4 u}{\partial x^4}\right]\right\} = 0,$$

$$(20)$$

in which "*" is dropped in Eqs. (19) and (20) for the sake of convenience.

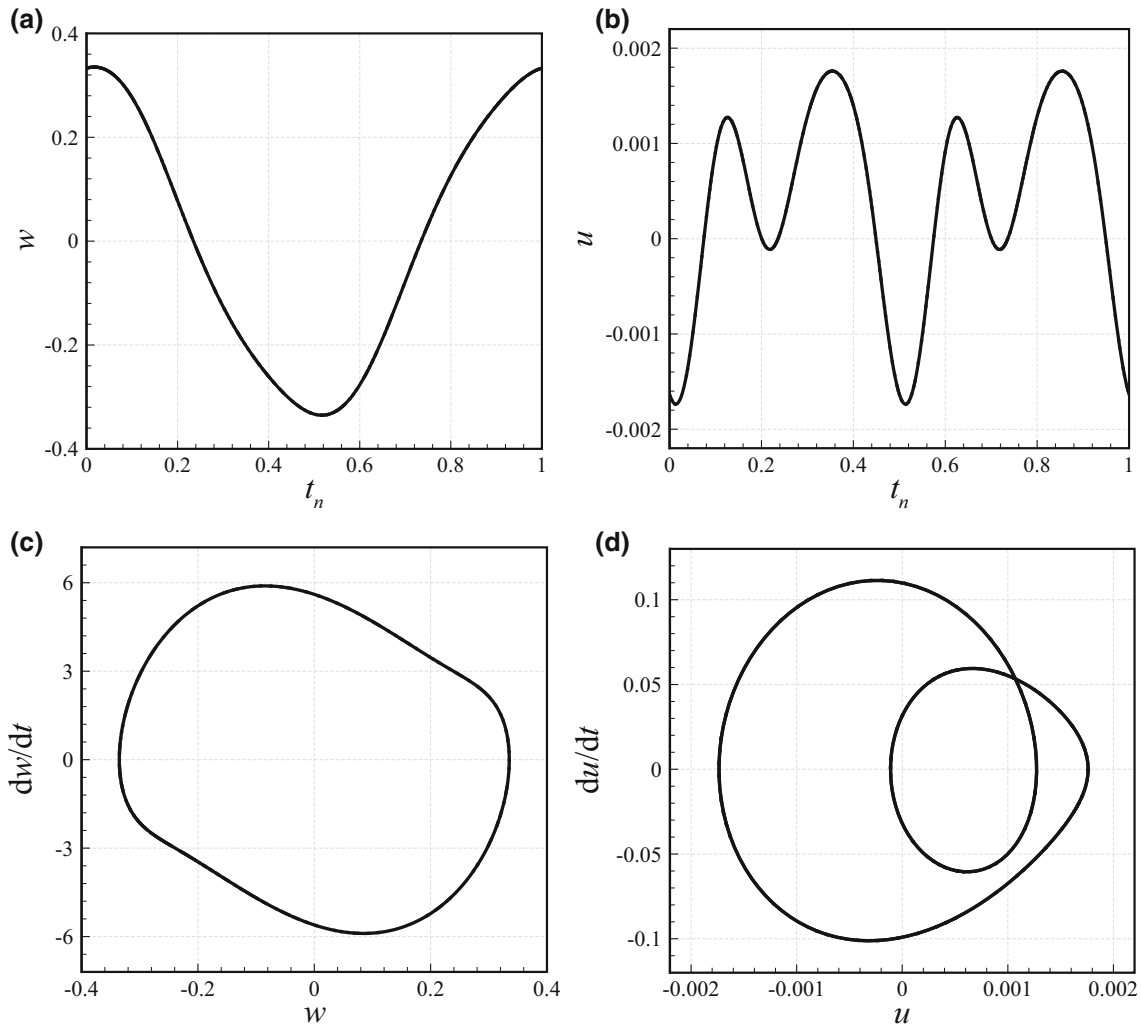**(a)**

(b)

(c)

(d)

Fig. 4 Detailed motion characteristics of the system of Fig. 2 at $\omega/\omega_1 = 1.0522$ (i.e. when the modal interactions are strongest). **a, b** w versus t_n for $x = 0.5$ and u versus t_n for $x = 0.657$, respectively; **c, d** dw/dt versus w for $x = 0.5$ and du/dt versus u for $x = 0.657$, respectively

3 Galerkin-based discretisation and solution technique

A Galerkin-based discretisation is performed in this section using the following expressions for the displacement components

$$\begin{Bmatrix} u \\ w \end{Bmatrix} = \begin{Bmatrix} \sum_{k=1}^{N_\zeta} r_k(t)\zeta_k(x) \\ \sum_{k=1}^{N_\eta} q_k(t)\eta_k(x) \end{Bmatrix}, \tag{21}$$

where r_k and q_k are generalised coordinates whereas ζ_k and η_k are trial functions (Ghayesh 2018b, c; Farokhi et al. 2017; Farajpour et al. 2018f; Ghayesh and Farokhi 2015b). Assuming clamped–clamped boundary conditions and using Eq. (21), one can obtain

$$\sum_{k=1}^{N_\zeta} \ddot{r}_k \left(\int_0^1 \zeta_i \zeta_k dx \right) + 2\kappa_v \sqrt{M} U \sum_{k=1}^{N_\zeta} \dot{r}_k \left(\int_0^1 \zeta_i (\zeta_k)' dx \right)$$

$$+ \kappa_v^2 U^2 \sum_{k=1}^{N_\zeta} r_k \left(\int_0^1 \zeta_i (\zeta_k)'' dx \right) - \chi_{nl}^2 \left[\sum_{k=1}^{N_\zeta} \ddot{r}_k \left(\int_0^1 \zeta_i (\zeta_k)'' dx \right) \right.$$

$$+ 2\kappa_v \sqrt{M} U \sum_{k=1}^{N_\zeta} \dot{r}_k \left(\int_0^1 \zeta_i (\zeta_k)''' dx \right) + \kappa_v^2 U^2 \sum_{k=1}^{N_\zeta} r_k \left(\int_0^1 \zeta_i (\zeta_k)'''' dx \right) \right]$$

$$- \Xi \left[\sum_{k=1}^{N_\zeta} r_k \left(\int_0^1 \zeta_i (\zeta_k)'' dx \right) + \frac{1}{s} \sum_{j=1}^{N_\eta} \sum_{k=1}^{N_\eta} q_k q_j \left(\int_0^1 \zeta_i (\eta_j)'' (\eta_k)' dx \right) \right]$$

$$+ \Xi \chi_{sg}^2 \left[\sum_{k=1}^{N_\zeta} r_k \left(\int_0^1 \zeta_i (\zeta_k)'''' dx \right) + \frac{3}{s} \sum_{j=1}^{N_\eta} \sum_{k=1}^{N_\eta} q_k q_j \left(\int_0^1 \zeta_i (\eta_j)''' (\eta_k)'' dx \right) \right.$$

$$+ \frac{1}{s} \sum_{j=1}^{N_\eta} \sum_{k=1}^{N_\eta} q_k q_j \left(\int_0^1 \zeta_i (\eta_j)'''' (\eta_k)' dx \right) \right] = 0, \tag{22}$$
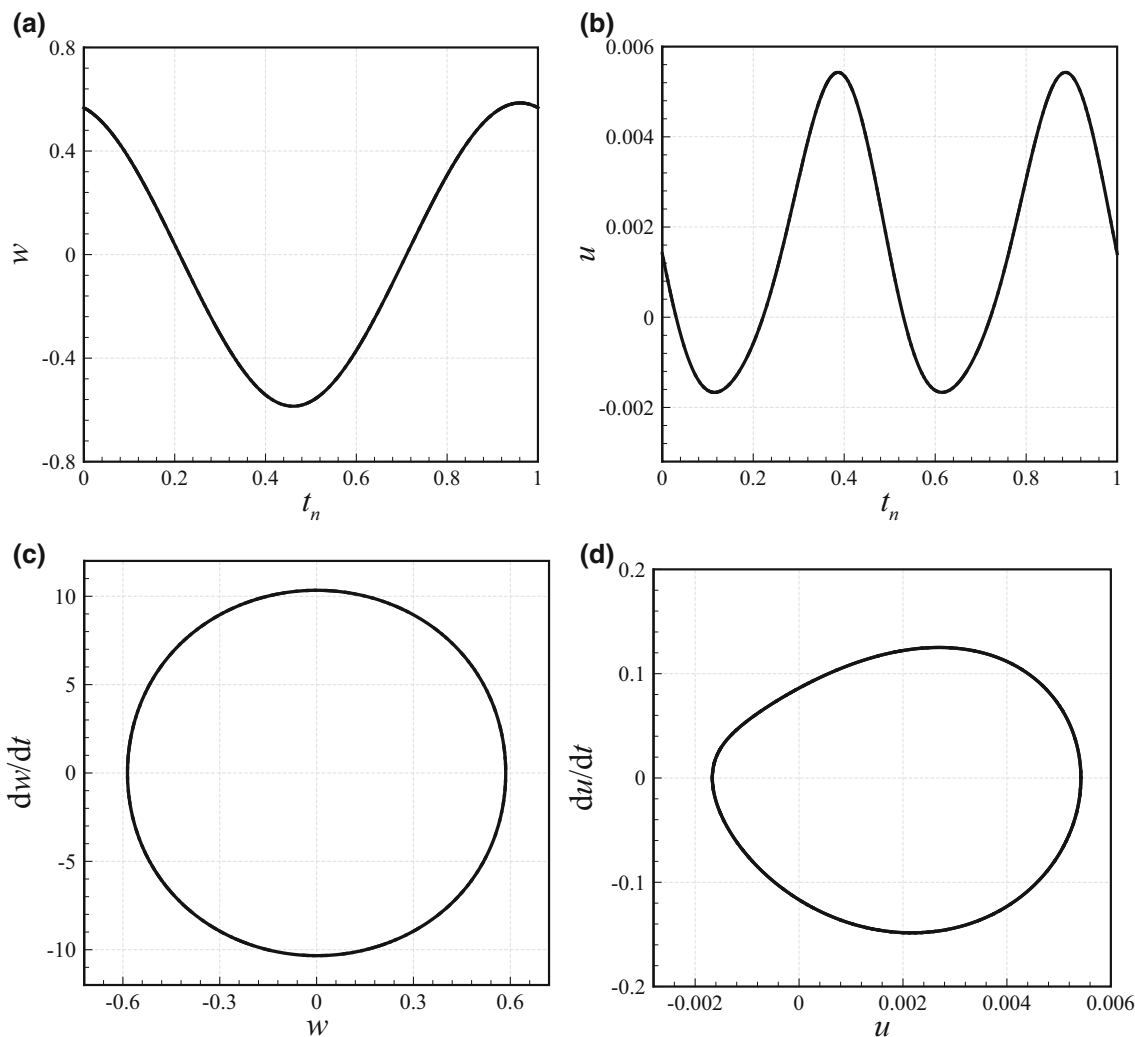
Fig. 5 Detailed motion characteristics of the system of Fig. 2 at $\omega/\omega_1 = 1.1608$ (i.e. at peak oscillation amplitude). **a**, **b** w versus t_n for $x = 0.5$ and u versus t_n for $x = 0.657$, respectively; **c**, **d** dw/dt versus w for $x = 0.5$ and du/dt versus u for $x = 0.657$, respectively

$$\sum_{k=1}^{N_\eta} \ddot{q}_k \left(\int_0^1 \eta_i \eta_k dx \right) + 2\kappa_v \sqrt{\bar{M}} U \sum_{k=1}^{N_\eta} \dot{q}_k \left(\int_0^1 \eta_i (\eta_k)' dx \right)$$

$$+ \kappa_v^2 U^2 \sum_{k=1}^{N_\eta} q_k \left(\int_0^1 \eta_i (\eta_k)'' dx \right) - \chi_{nl}^2 \left[\sum_{k=1}^{N_\eta} \ddot{q}_k \left(\int_0^1 \eta_i (\eta_k)'' dx \right) \right.$$

$$+ 2\kappa_v \sqrt{\bar{M}} U \sum_{k=1}^{N_\eta} \dot{q}_k \left(\int_0^1 \eta_i (\eta_k)''' dx \right) + \kappa_v^2 U^2 \sum_{k=1}^{N_\eta} q_k \left(\int_0^1 \eta_i (\eta_k)'''' dx \right) \Bigg]$$

$$+ \sum_{k=1}^{N_\eta} q_k \left(\int_0^1 \eta_i (\eta_k)'''' dx \right) - \chi_{sg}^2 \sum_{k=1}^{N_\eta} q_k \left(\int_0^1 \eta_i (\eta_k)^{(6)} dx \right)$$

$$- \left(\int_0^1 \eta_i dx \right) F_1 \cos(\omega t) - \frac{\Xi}{s^2} \left\{ s \sum_{k=1}^{N_\zeta} \sum_{l=1}^{N_\eta} q_l r_k \left(\int_0^1 \eta_i (\zeta_k)' (\eta_l)'' dx \right) \right.$$

$$+ \frac{1}{2} \sum_{j=1}^{N_\zeta} \sum_{k=1}^{N_\zeta} \sum_{l=1}^{N_\eta} q_l r_k r_j \left(\int_0^1 \eta_i (\eta_j)' (\eta_k)' (\eta_l)'' dx \right)$$

$$+ s \sum_{k=1}^{N_\zeta} \sum_{l=1}^{N_\eta} q_l r_k \left(\int_0^1 \eta_i (\zeta_k)'' (\eta_l)' dx \right)$$

$$+ \sum_{j=1}^{N_\eta} \sum_{k=1}^{N_\eta} \sum_{l=1}^{N_\eta} q_l q_k q_j \left(\int_0^1 \eta_i (\eta_j)'' (\eta_k)' (\eta_l)' dx \right)$$

$$- \chi_{sg}^2 \left[s \sum_{k=1}^{N_\zeta} \sum_{l=1}^{N_\eta} q_l r_k \left(\int_0^1 \eta_i (\zeta_k)''' (\eta_l)'' dx \right) \right.$$

$$+ \sum_{l=1}^{N_\eta} \sum_{j=1}^{N_\eta} \sum_{k=1}^{N_\eta} q_k q_j q_l \left(\int_0^1 \eta_i (\eta_l)'' (\eta_j)'' (\eta_k)'' dx \right)$$

$$+ \sum_{l=1}^{N_\eta} \sum_{j=1}^{N_\eta} \sum_{k=1}^{N_\eta} q_k q_j q_l \left(\int_0^1 \eta_i (\eta_l)'' (\eta_j)''' (\eta_k)' dx \right) \Bigg]$$
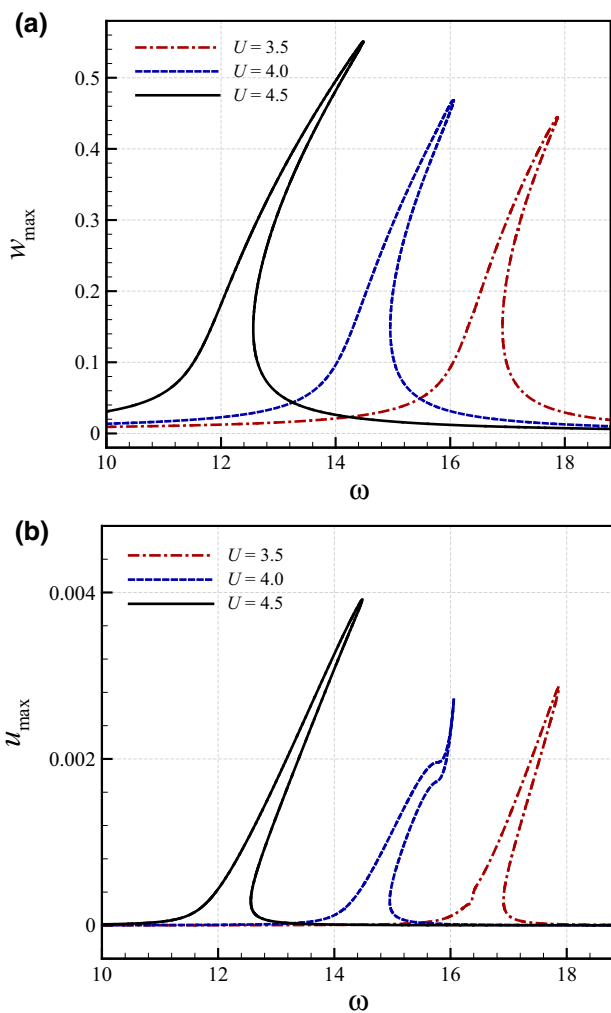
Fig. 6 Change of maximum transverse and axial displacements versus the excitation frequency for different fluid speeds in subcritical flow regime; **a** w_{max} at $x = 0.5$; **b** u_{max} at $x = 0.657$
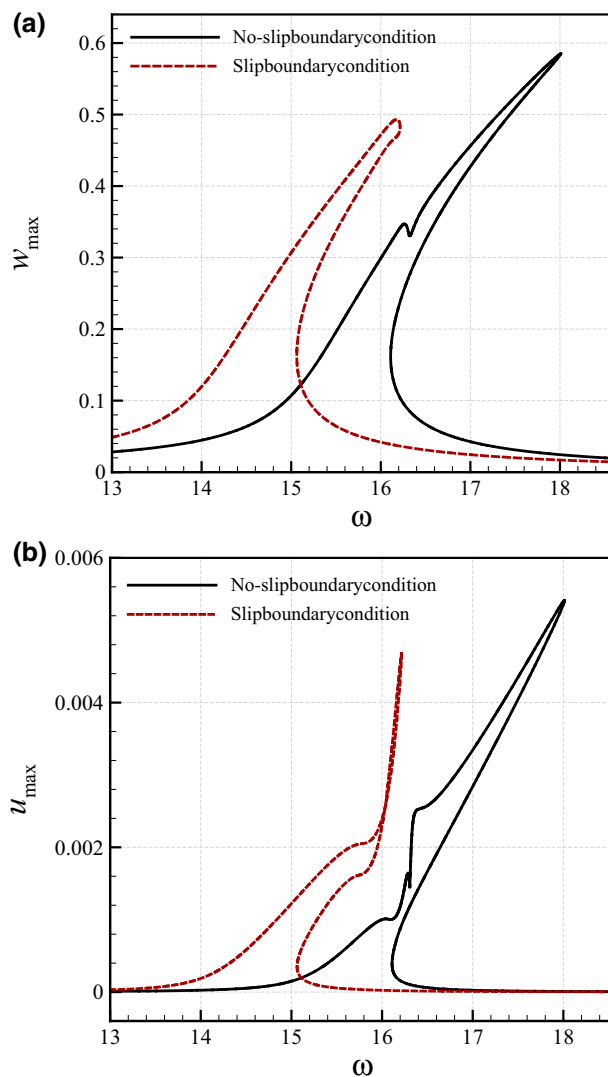

Fig. 7 Effects of slip boundary conditions on the forced oscillation when $U = 3.5$ (subcritical flow regime); **a** w_{max} at $x = 0.5$; **b** u_{max} at $x = 0.657$

$$-\chi_{sg}^2 \left[s \sum_{l=1}^{N_\eta} \sum_{k=1}^{N_\zeta} r_k q_l \left(\int_0^1 \eta_i (\eta_l)' (\zeta_k)'''' dx \right) \right.$$

$$+3 \sum_{j=1}^{N_\eta} \sum_{k=1}^{N_\eta} \sum_{l=1}^{N_\eta} q_l q_k q_j \left(\int_0^1 \eta_i (\eta_j)''' (\eta_k)'' (\eta_l)' dx \right)$$

$$+ \sum_{l=1}^{N_\eta} \sum_{j=1}^{N_\eta} \sum_{k=1}^{N_\eta} q_k q_j q_l \left(\int_0^1 \eta_i (\eta_l)' (\eta_j)'''' (\eta_k)' dx \right) \right]$$

$$+ \frac{s\chi_{nl}^2}{\Xi} \left[\sum_{k=1}^{N_\zeta} \sum_{l=1}^{N_\eta} q_l \ddot{r}_k \left(\int_0^1 \eta_i (\zeta_k)' (\eta_l)'' dx \right) \right.$$

$$+\kappa_v^2 U^2 \sum_{k=1}^{N_\zeta} \sum_{l=1}^{N_\eta} q_l r_k \left(\int_0^1 \eta_i (\zeta_k)''' (\eta_l)'' dx \right)$$

$$+2\kappa_v \sqrt{\overline{M}} U \sum_{k=1}^{N_\zeta} \sum_{l=1}^{N_\eta} q_l \dot{r}_k \left(\int_0^1 \eta_i (\zeta_k)'' (\eta_l)'' dx \right) \right]$$

$$+ \frac{s\chi_{nl}^2}{\Xi} \left[\sum_{l=1}^{N_\eta} \sum_{k=1}^{N_\zeta} \ddot{r}_k q_l \left(\int_0^1 \eta_i (\eta_l)' (\zeta_k)'' dx \right) \right.$$

$$+\kappa_v^2 U^2 \sum_{k=1}^{N_\zeta} \sum_{l=1}^{N_\eta} q_l r_k \left(\int_0^1 \eta_i (\zeta_k)'''' (\eta_l)' dx \right) + 2\kappa_v \sqrt{\overline{M}} U \sum_{l=1}^{N_\eta} \sum_{k=1}^{N_\zeta} \dot{r}_k$$

$$\times q_l \left(\int_0^1 \eta_i (\eta_l)' (\zeta_k)''' dx \right) \right] \right\}$$

$$+ \frac{\Xi\chi_{nl}^2}{s^2} \int_0^1 \left\{ \eta_i \left[s \sum_{k=1}^{N_\zeta} \sum_{l=1}^{N_\eta} q_l r_k (\zeta_k)'' (\eta_l)' + \sum_{j=1}^{N_\eta} \sum_{k=1}^{N_\eta} \sum_{l=1}^{N_\eta} q_l q_k q_j (\eta_j)'' (\eta_k)' (\eta_l)' \right. \right.$$
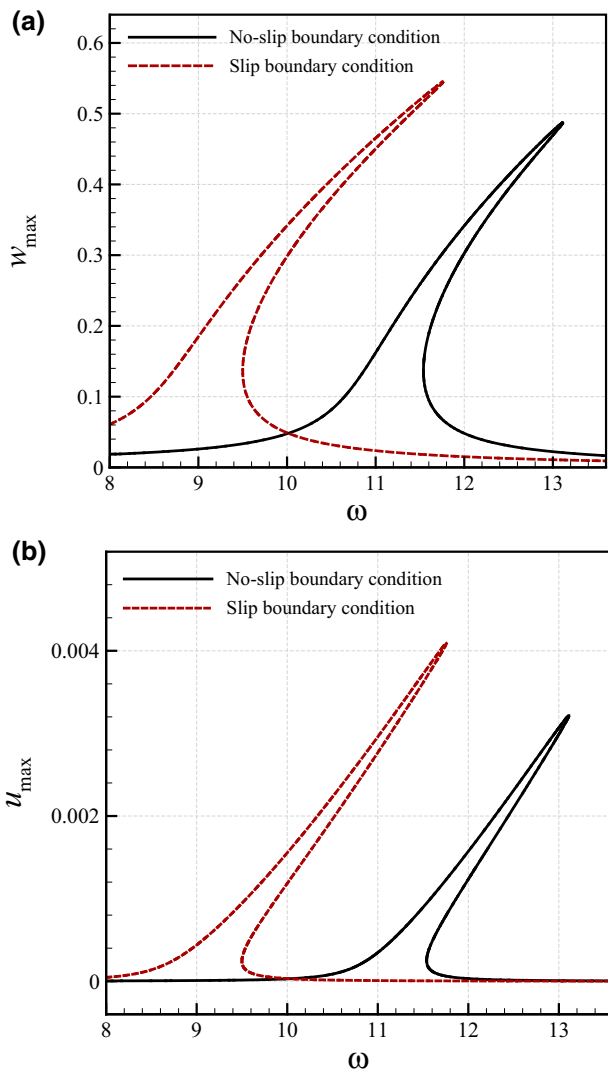
Fig. 8 Effects of slip boundary conditions on the forced oscillation when $U = 4.5$ (subcritical flow regime); **a** w_{max} at $x = 0.5$; **b** u_{max} at $x = 0.657$
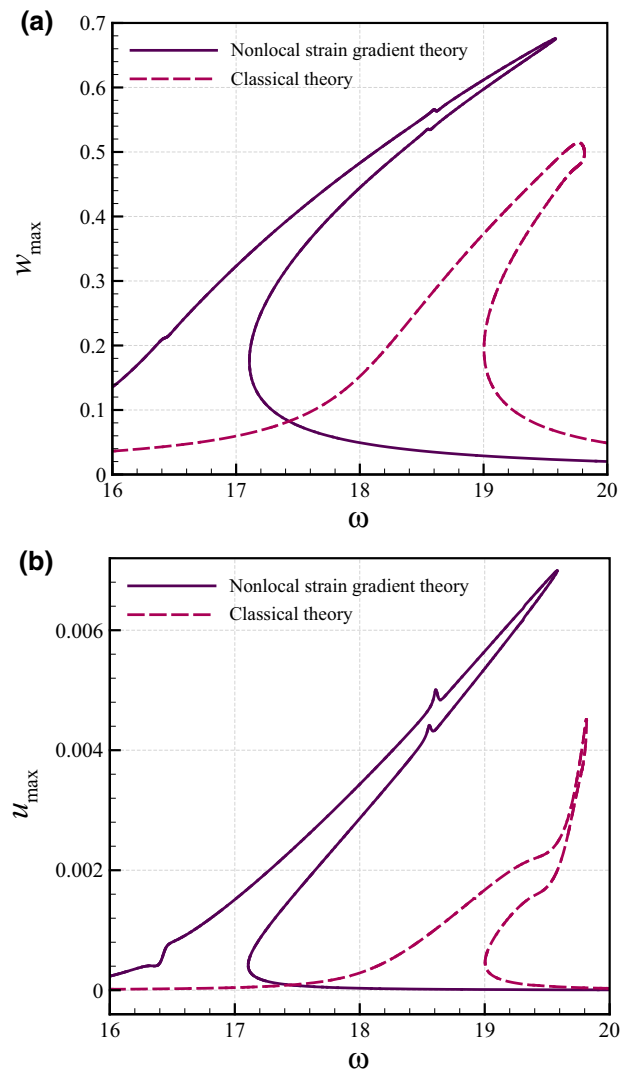
Fig. 9 Change of maximum transverse and axial displacements versus the excitation frequency obtained via the nonlocal strain gradient theory and classical theory for $U = 3.0$ (subcritical flow regime); **a** w_{max} at $x = 0.5$; **b** u_{max} at $x = 0.657$

$$+ s \sum_{k=1}^{N_\zeta} \sum_{l=1}^{N_\eta} q_l r_k (\zeta_k)' (\eta_l)'' + \frac{1}{2} \sum_{j=1}^{N_\zeta} \sum_{k=1}^{N_\zeta} \sum_{l=1}^{N_\eta} q_l r_k r_j (\eta_j)' (\eta_k)' (\eta_l)''$$

$$- \chi_{sg}^2 \left(s \sum_{k=1}^{N_\zeta} \sum_{l=1}^{N_\eta} q_l r_k (\zeta_k)''' (\eta_l)'' + \sum_{l=1}^{N_\eta} \sum_{j=1}^{N_\eta} \sum_{k=1}^{N_\eta} q_k q_j q_l (\eta_l)'' (\eta_j)'' (\eta_k)'' \right.$$

$$+ \sum_{l=1}^{N_\eta} \sum_{j=1}^{N_\eta} \sum_{k=1}^{N_\eta} q_k q_j q_l (\eta_l)'' (\eta_j)''' (\eta_k)' \right) - \chi_{sg}^2 \left(s \sum_{l=1}^{N_\eta} \sum_{k=1}^{N_\zeta} r_k q_l (\eta_l)' (\zeta_k)'''' \right.$$

$$+ 3 \sum_{j=1}^{N_\eta} \sum_{k=1}^{N_\eta} \sum_{l=1}^{N_\eta} q_l q_k q_j (\eta_j)''' (\eta_k)'' (\eta_l)' + \sum_{l=1}^{N_\eta} \sum_{j=1}^{N_\eta} \sum_{k=1}^{N_\eta} q_k q_j q_l (\eta_l)' (\eta_j)'''' (\eta_k)' \right)$$

$$+ \frac{s \chi_{nl}^2}{\Xi} \left(\sum_{k=1}^{N_\zeta} \sum_{l=1}^{N_\eta} q_l \ddot{r}_k (\zeta_k)' (\eta_l)'' + 2\kappa_v \sqrt{\bar{M}} U \sum_{k=1}^{N_\zeta} \sum_{l=1}^{N_\eta} q_l \dot{r}_k (\zeta_k)'' (\eta_l)'' \right.$$

$$+ \kappa_v^2 U^2 \sum_{k=1}^{N_\zeta} \sum_{l=1}^{N_\eta} q_l r_k (\zeta_k)''' (\eta_l)'' \right) + \frac{s \chi_{nl}^2}{\Xi} \left(\sum_{l=1}^{N_\eta} \sum_{k=1}^{N_\zeta} \ddot{r}_k q_l (\eta_l)' (\zeta_k)''' + 2\kappa_v \sqrt{\bar{M}} U \right.$$

$$\left. \left. \times \sum_{l=1}^{N_\eta} \sum_{k=1}^{N_\zeta} \dot{r}_k q_l (\eta_l)' (\zeta_k)'''' + \kappa_v^2 U^2 \sum_{k=1}^{N_\zeta} \sum_{l=1}^{N_\eta} q_l r_k (\zeta_k)'''' (\eta_l)'' \right] \right)'' \right\} dx = 0.$$

$$\tag{23}$$

Equations (22) and (23) indicate a set of time-dependent ordinary differential equations, which can be solved via a continuation approach. It is worth mentioning that for developing a numerical solution, ten trial functions are assumed.
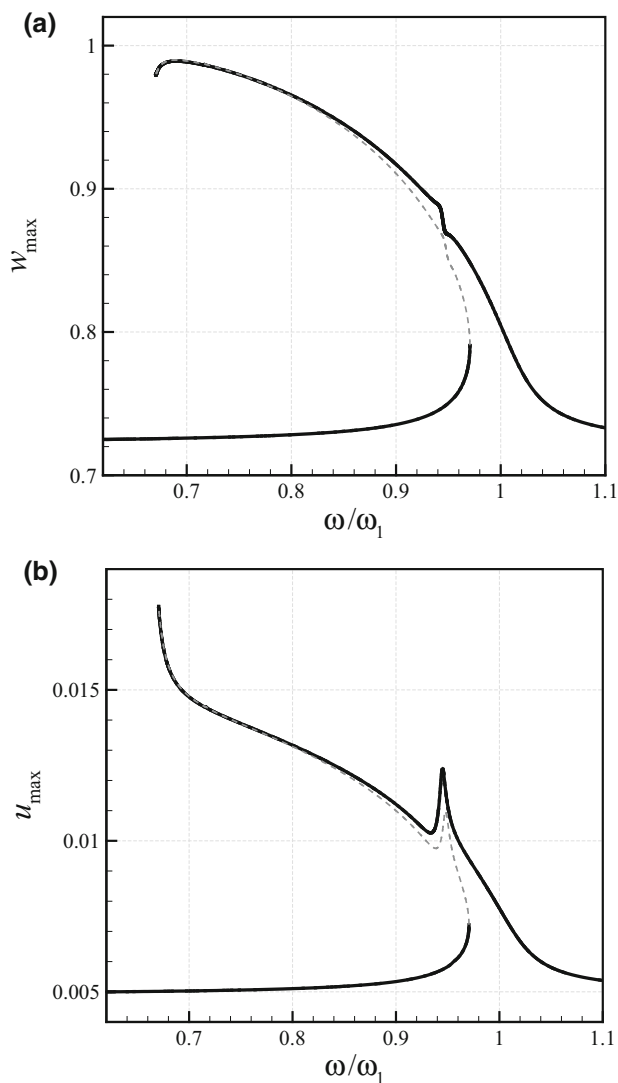
(a)

(b)

Fig. 10 Change of maximum transverse and axial displacements versus the excitation frequency in the supercritical flow regime; **a** w_{max} at $x = 0.5$; **b** u_{max} at $x = 0.657$

4 Results and discussion

For constructing the frequency-response curves of the fluid-conveying nanosystem incorporating both stress nonlocality and strain gradients, the tube material and geometrical parameters are assumed as $\rho = 1024$ kg/m^3, $v = 0.3$, $E = 610$ MPa, $h = 66.0$ nm and $R_o = 290.5$ nm where h, ρ and R_o are respectively the nanotube thickness, density and outer radius. In the numerical solution, a dimensionless damping coefficient of 0.25 is added for both u and w motions. The focus of this paper is not on the influence of viscoelastic medium. The system dimensionless parameters are $\kappa_v = 1.0788$, $\bar{M} = 0.5915$, $\chi_{sg} = 0.04$, $\chi_{nl} = 0.09$, $\Xi = 4006.9411$ and $s = 20.0$, unless otherwise specifically mentioned.

The change of maximum transverse and axial displacements versus the frequency ratio (the ratio of excitation frequency to fundamental natural one) is plotted in Fig. 2 for $F_1 = 2.0$ and $U = 3.25$. The flow regime is subcritical since the flow speed is less than the critical one associated with buckling ($U_{cr} = 5.1862$). Both unstable and stable branches are indicated in the figure. Two bifurcation points at $\omega/\omega_1 = 1.1608$ and 1.0378 are seen for the fluid-conveying nanosystem. Moreover, it is found that the nonlinearity of the nanosystem is of hardening type. In addition, modal interactions are found in the nonlinear response.

In order to study the modal interaction in the nonlinear dynamics of the fluid-conveying nanosystem, the change of first four generalised coordinates of the transverse motion versus the frequency ratio is plotted in Fig. 3. Strong modal interactions as well as energy transfer between modes are observed in the nonlinear response of the nanosystem, especially for higher generalised coordinates.

The detailed motion characteristics of the nanotube of Fig. 2 are shown in Figs. 4 and 5 for $\omega/\omega_1 = 1.0522$ and $\omega/\omega_1 = 1.1608$, respectively; the former case is the one when the modal interactions are strongest. Time histories and phase-plane plots for both types of motions are plotted. It should be noticed that t_n denotes normalised time with respect to the period of oscillation. It can be concluded that in the presence of strong modal interactions, the motion characteristics of the nanotube are different, especially for the axial motion.

The change of maximum transverse and axial displacements versus the excitation frequency is plotted in Fig. 6 for various fluid speeds in the subcritical regime. The forcing amplitude, speed correction factor, nonlocal coefficient and strain gradient coefficient are set to $F_1 = 1.5$, $\kappa_s = 1.0788$, $\chi_{nl} = 0.09$, and $\chi_{sg} = 0.04$, respectively. It is found that higher fluid speeds yield higher peak amplitudes but lower resonance frequencies for both motion types of the fluid-conveying nanosystem.

Figure 7 is plotted for comparing the nanosystem frequency response for slip conditions with that calculated using no-slip boundary conditions. The forcing amplitude, speed correction factor, fluid speed, nonlocal coefficient and strain gradient coefficient are set to $F_1 = 2$, $\kappa_{s-} = 1.0788$, $U = 3.5$, $\chi_{nl} = 0.09$, and $\chi_{sg} = 0.04$, respectively. The no-slip condition yields overestimated results for both resonance frequency and peak amplitude of the nanotube. Figure 8 also compares the slip and no-slip boundary conditions for a higher fluid speed ($U = 4.5$) in the subcritical regime. The amplitude of the external distributed loading is $F_1 = 1.2$. Comparing Figs. 7 and 8 indicates that the effect of slip conditions on the subcritical frequency response increases as the flow speed increases.
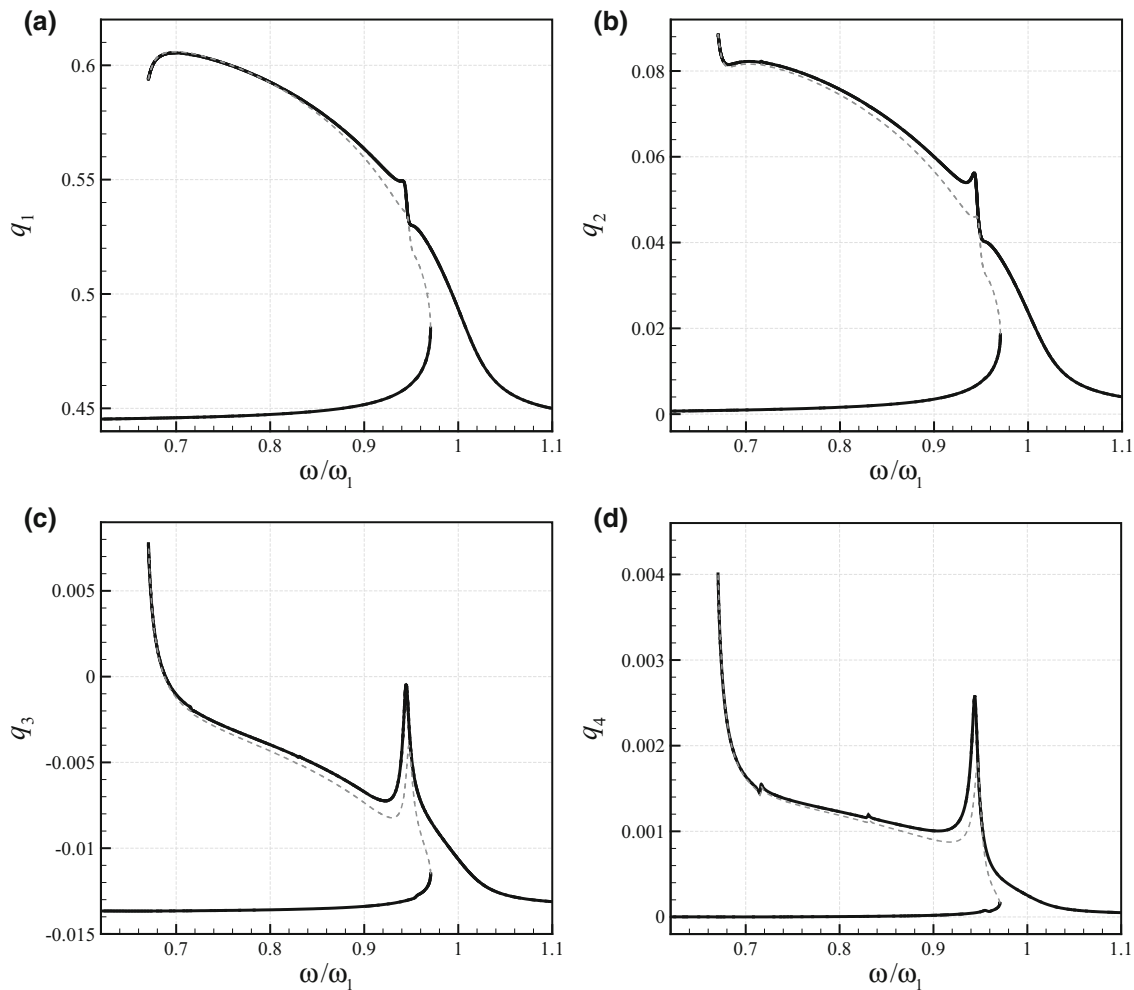
Fig. 11 Change of **a** q_1, **b** q_2, **c** q_3 and **d** q_4 versus the ratio of the excitation frequency to the natural one in the supercritical flow regime

The change of maximum transverse and axial displacements versus the excitation frequency is plotted in Fig. 9 for both the classical theory of beams and the NSGT-based model. For the classical theory of beams, both scale coefficients are zero (i.e. $\chi_{nl} = \chi_{sg} = 0$) whereas the scale coefficients are as $\chi_{nl} = 0.09$, $\chi_{sg} = 0.04$ for the NSGT-based model. The speed correction factor and forcing amplitude are $\kappa_s = 1.0788$ and $F_1 = 2.5$, respectively. The NSGT yields a relatively high peak amplitude but a low resonance frequency, compared to the classical theory. This is due to the high value of nonlocal coefficient compared to the strain gradient coefficient. In fact, since nonlocal effects are dominant for this case, the total structural stiffness of NSGT nanotubes is less than that calculated via the classical theory. This results in a lower resonance frequency as well as a higher peak amplitude for the nanosystem.

Figure 10 illustrates the change of maximum transverse and axial displacements versus the frequency ratio for

$F_1 = 1.0$, $U = 6.15$, $\kappa_s = 1.0788$, $\chi_{nl} = 0.09$, and $\chi_{sg} = 0.04$; the fundamental frequency is $\omega_1 = 12.9072$. It should be noticed that this time, the fluid speed is higher than the critical one (i.e. supercritical regime). The frequency response is of softening type containing two bifurcation points at $\omega/\omega_1 = 0.9706$ and 0.6705. This is in contrast to the subcritical frequency response in which a hardening nonlinearity is observed. Moreover, modal interactions are found in the nonlinear response for both motion types. Figure 11 gives the frequency response of the tube for the first four generalised coordinates. Strong modal interactions as well as energy transfer between modes are observed in the nonlinear response, especially for higher generalised coordinates. Furthermore, the detailed motion characteristics of the nanosystem of Fig. 10 at $\omega/\omega_1 = 0.6705$ (i.e. at peak oscillation amplitude) are indicated in Fig. 12; phase-plane plots and time histories for both motion types are shown.
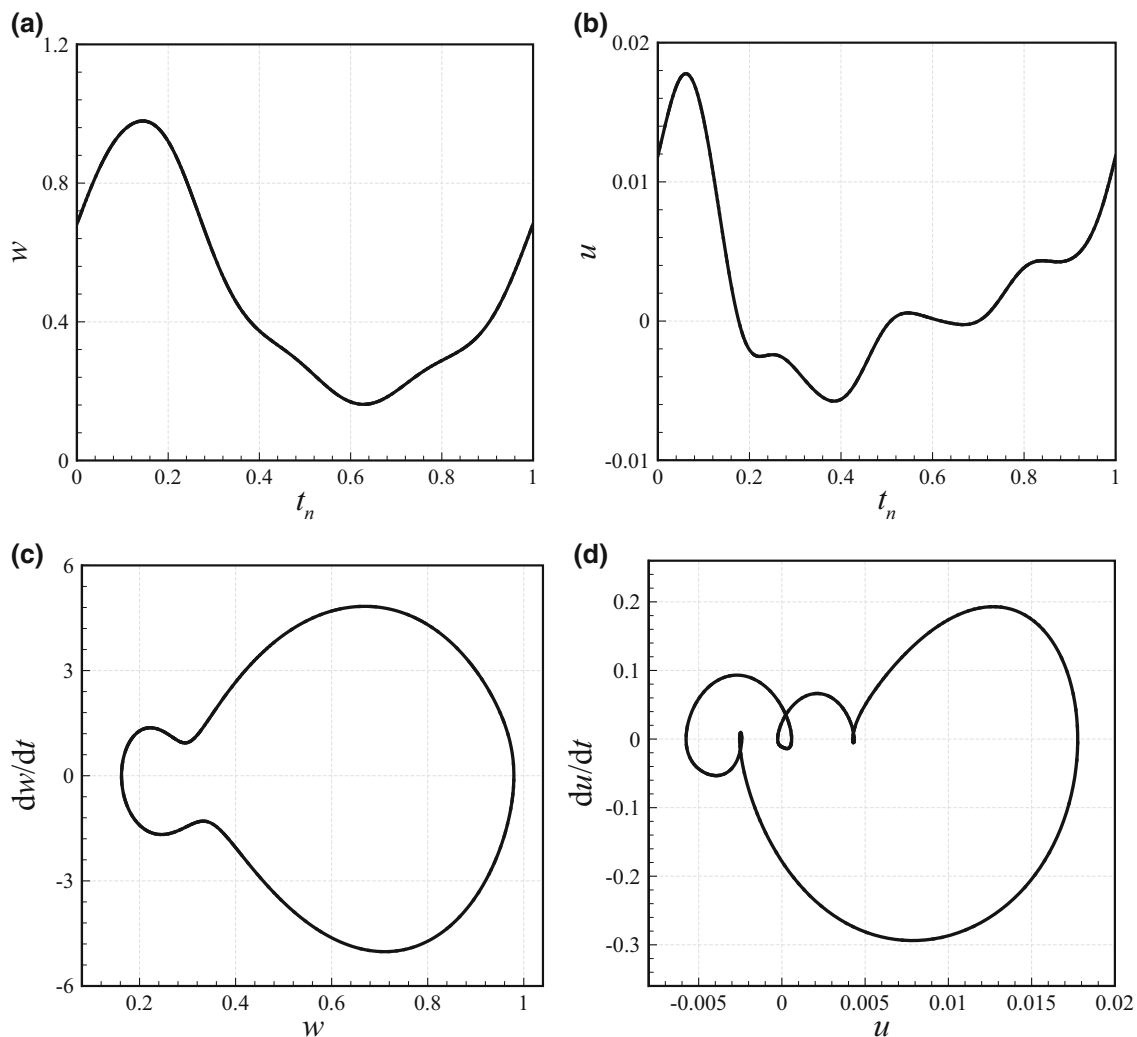
Fig. 12 Detailed motion characteristics of the nanosystem of Fig. 10 at $\omega/\omega_1 = 0.6705$. **a**, **b** w versus t_n for $x = 0.5$ and u versus t_n for $x = 0.657$, respectively; **c**, **d** dw/dt versus w for $x = 0.5$ and du/dt versus u for $x = 0.657$, respectively

Figure 13 depicts the change of maximum transverse and axial displacements versus the frequency ratio for $F_1 = 1.0$, $\kappa_s = 1.0788$, $\chi_{nl} = 0.09$, and $\chi_{sg} = 0.04$. In contrast to the subcritical regime in which increasing U decreases natural frequency, in supercritical regime increasing U increases natural frequency (shifts frequency response to the right). Figure 14 compares the frequency responses using no-slip and slip conditions in the supercritical regimes for $\chi_{nl} = 0.09$, $\chi_{sg} = 0.04$, and $F_1 = 0.8$. The no-slip condition underestimates both peak amplitude and resonance frequency in the supercritical regime. This is in contrast to the subcritical frequency response in which the no-slip condition yields overestimated results for both the resonance frequency and peak amplitude.

5 Conclusions

The large-amplitude forced oscillations of nanotubes conveying fluid were analysed via a size-dependent coupled nonlinear model of beams. The proposed model contained two different size parameters, leading to a better simulation of size effects on the nonlinear oscillations. Both axial and transverse inertial terms were taken into consideration. To incorporate the mean free path of molecules at the tube/fluid interface, the Beskok–Karniadakis approach was implemented. The coupled nonlinear equations were finally obtained, discretised and solved via application of the NSGT, Galerkin's technique and continuation method, respectively.

In the supercritical flow regime, the frequency response is of softening type containing two saddle-node bifurcations while the subcritical frequency response is of a
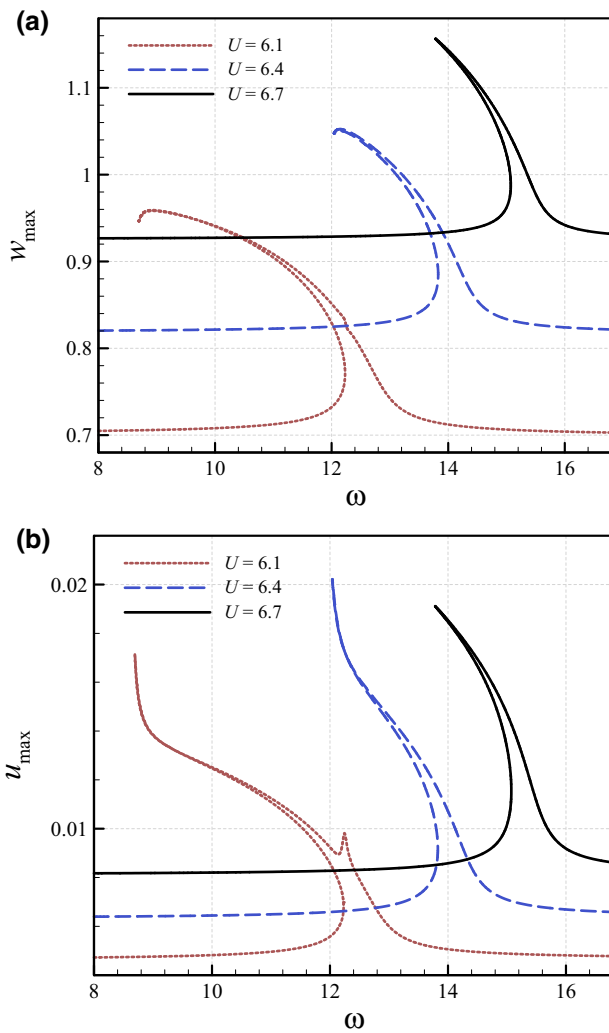
Fig. 13 Change of maximum transverse and axial displacements versus the excitation frequency for different fluid speeds in supercritical flow regime; **a** w_{max} at $x = 0.5$; **b** u_{max} at $x = 0.657$

hardening nonlinearity. When nonlocal influences are dominant, the total stiffness of NSGT nanotubes is less, and this leads to a lower resonance frequency and a higher peak amplitude for the nanosystem conveying fluid. Strong modal interactions as well as energy transfer between modes are observed in both flow regimes. In contrast to the subcritical regime in which higher fluid speeds yield a decrease in the natural frequency, in supercritical regime, the natural frequency increases with increasing fluid speed. Furthermore, no-slip boundary conditions lead to underestimated supercritical peak amplitudes and resonance frequencies for the NSGT nanotube whereas no-slip boundary conditions yield overestimated subcritical resonance frequencies and peak amplitudes.
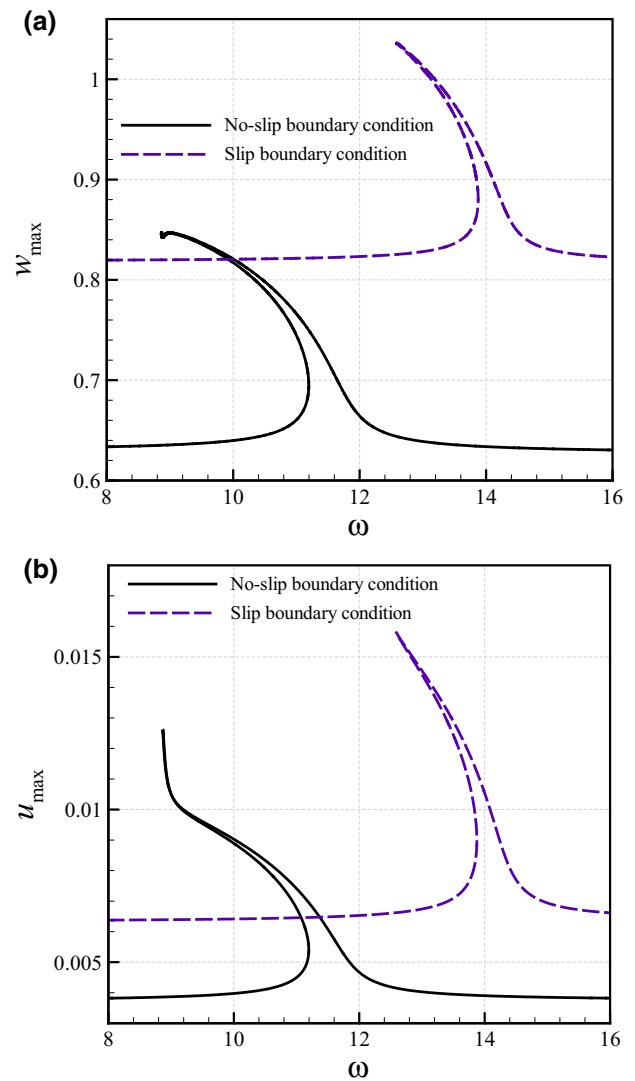

Fig. 14 Effects of slip boundary conditions on the forced oscillation when $U = 6.4$ (supercritical flow regime); **a** w_{max} at $x = 0.5$; **b** u_{max} at $x = 0.657$

References

Akgöz B, Civalek Ö (2011) Buckling analysis of cantilever carbon nanotubes using the strain gradient elasticity and modified couple stress theories. J Comput Theor Nanosci 8:1821–1827

Ansari R, Norouzzadeh A, Gholami R, Shojaei MF, Darabi M (2016) Geometrically nonlinear free vibration and instability of fluid-conveying nanoscale pipes including surface stress effects. Microfluid Nanofluid 20:28

Aydogdu M (2014) Longitudinal wave propagation in multiwalled carbon nanotubes. Compos Struct 107:578–584

Aydogdu M, Filiz S (2011) Modeling carbon nanotube-based mass sensors using axial vibration and nonlocal elasticity. Phys Low Dimens Syst Nanostruct 43:1229–1234

Babaei A, Yang CX (2019) Vibration analysis of rotating rods based on the nonlocal elasticity theory and coupled displacement field. Microsys Technol 25:1077–1085. https://doi.org/10.1007/s00542-018-4047-3

Beskok A, Karniadakis GE (1999) Report: a model for flows in channels, pipes, and ducts at micro and nano scales. Microscale Thermophys Eng 3:43–77

Dai H, Wang L, Abdelkefi A, Ni Q (2015) On nonlinear behavior and buckling of fluid-transporting nanotubes. Int J Eng Sci 87:13–22

De Volder MF, Tawfick SH, Baughman RH, Hart AJ (2013) Carbon nanotubes: present and future commercial applications. Science 339:535–539

Ebrahimi F, Barati MR (2019) Dynamic modeling of embedded nanoplate systems incorporating flexoelectricity and surface effects. Microsys Technol 25:175–187. https://doi.org/10.1007/s00542-018-3946-7

Farajpour A, Rastgoo A, Farajpour M (2017) Nonlinear buckling analysis of magneto-electro-elastic CNT-MT hybrid nanoshells based on the nonlocal continuum mechanics. Compos Struct 180:179–191

Farajpour A, Ghayesh MH, Farokhi H (2018a) A review on the mechanics of nanostructures. Int J Eng Sci 133:231–263

Farajpour M, Shahidi A, Tabataba'i-Nasab F, Farajpour A (2018b) Vibration of initially stressed carbon nanotubes under magneto-thermal environment for nanoparticle delivery via higher-order nonlocal strain gradient theory. Eur Phys J Plus 133:219

Farajpour MR, Shahidi A, Farajpour A (2018c) Resonant frequency tuning of nanobeams by piezoelectric nanowires under thermo-electro-magnetic field: a theoretical study. Micro Nano Lett 13:1627–1632

Farajpour MR, Shahidi A, Farajpour A (2018d) A nonlocal continuum model for the biaxial buckling analysis of composite nanoplates with shape memory alloy nanowires. Mater Res Expr 5:035026

Farajpour MR, Shahidi A, Hadi A, Farajpour A (2018e) Influence of initial edge displacement on the nonlinear vibration, electrical and magnetic instabilities of magneto-electro-elastic nanofilms. Mech Adv Mat Struct. https://doi.org/10.1080/15376494.2018.1432820

Farajpour A, Farokhi H, Ghayesh MH, Hussain S (2018f) Nonlinear mechanics of nanotubes conveying fluid. Int J Eng Sci 133:132–143

Farajpour A, Ghayesh MH, Farokhi H (2019a) Large-amplitude coupled scale-dependent behaviour of geometrically imperfect NSGT nanotubes. Int J Mech Sci 150:510–525

Farajpour A, Ghayesh MH, Farokhi H (2019b) Application of nanotubes in conveying nanofluid: a bifurcation analysis with consideration of internal energy loss and geometrical imperfection. Microsyst Technol. https://doi.org/10.1007/s00542-019-04344-z

Farokhi H, Ghayesh MH (2015) Nonlinear dynamical behaviour of geometrically imperfect microplates based on modified couple stress theory. Int J Mech Sci 90:133–144

Farokhi H, Ghayesh MH (2016) Size-dependent behaviour of electrically actuated microcantilever-based MEMS. Int J Mech Mater Des 12:301–315

Farokhi H, Ghayesh MH (2018) Nonlinear mechanics of electrically actuated microplates. Int J Eng Sci 123:197–213. https://doi.org/10.1016/j.ijengsci.2017.08.017

Farokhi H, Ghayesh MH, Gholipour A, Hussain S (2017) Motion characteristics of bilayered extensible Timoshenko microbeams. Int J Eng Sci 112:1–17

Farokhi H, Ghayesh MH, Gholipour A, Tavallaeinejad M (2018a) Stability and nonlinear dynamical analysis of functionally graded microplates. Microsyst Technol 24:2109–2121. https://doi.org/10.1007/s00542-018-3849-7

Farokhi H, Païdoussis MP, Misra AK (2018b) Nonlinear behaviour and mass detection sensitivity of geometrically imperfect cantilevered carbon nanotube resonators. Commun Nonlinear Sci Numer Simul 65:272–298

Ghayesh MH (2018a) Stability and bifurcation characteristics of viscoelastic microcantilevers. Microsyst Technol 24:4739–4746. https://doi.org/10.1007/s00542-018-3860-z

Ghayesh MH (2018b) Functionally graded microbeams: simultaneous presence of imperfection and viscoelasticity. Int J Mech Sci 140:339–350

Ghayesh MH (2018c) Dynamics of functionally graded viscoelastic microbeams. Int J Eng Sci 124:115–131

Ghayesh MH (2019) Viscoelastically coupled dynamics of FG Timoshenko microbeams. Microsyst Technol 25:651–663. https://doi.org/10.1007/s00542-018-4002-3

Ghayesh MH, Farokhi H (2015a) Nonlinear dynamics of microplates. Int J Eng Sci 86:60–73

Ghayesh MH, Farokhi H (2015b) Chaotic motion of a parametrically excited microbeam. Int J Eng Sci 96:34–45

Ghayesh MH, Farajpour A (2018a) Nonlinear mechanics of nanoscale tubes via nonlocal strain gradient theory. Int J Eng Sci 129:84–95

Ghayesh MH, Farajpour A (2018b) Vibrations of shear deformable FG viscoelastic microbeams. Microsystem Technol. https://doi.org/10.1007/s00542-00018-04184-00548

Ghayesh MH, Farajpour A (2019) A review on the mechanics of functionally graded nanoscale and microscale structures. Int J Eng Sci 137:8–36

Ghayesh MH, Farokhi H, Farajpour A (2019) Global dynamics of fluid conveying nanotubes. Int J Eng Sci 135:37–57

Ghayesh MH, Farokhi H (2018) Nonlinear behaviour of electrically actuated microplate-based MEMS resonators. Mech Syst Signal Process 109:220–234

Ghayesh MH, Amabili M, Farokhi H (2013a) Coupled global dynamics of an axially moving viscoelastic beam. Int J Non-Linear Mech 51:54–74

Ghayesh MH, Amabili M, Farokhi H (2013b) Nonlinear forced vibrations of a microbeam based on the strain gradient elasticity theory. Int J Eng Sci 63:52–60

Ghayesh MH, Farokhi H, Hussain S (2016a) Viscoelastically coupled size-dependent dynamics of microbeams. Int J Eng Sci 109:243–255

Ghayesh MH, Farokhi H, Alici G (2016b) Size-dependent performance of microgyroscopes. Int J Eng Sci 100:99–111

Ghayesh MH, Farokhi H, Farajpour A (2018) Chaotic oscillations of viscoelastic microtubes conveying pulsatile fluid. Microfluid Nanofluid 22:72

Ghayesh MH, Moradian N (2011) Nonlinear dynamic response of axially moving, stretched viscoelastic strings. Arch Appl Mech 81:781–799

Gholipour A, Farokhi H, Ghayesh MH (2015) In-plane and out-of-plane nonlinear size-dependent dynamics of microplates. Nonlin Dynam 79:1771–1785

Gholipour A, Ghayesh MH, Zander A (2018a) Nonlinear biomechanics of bifurcated atherosclerotic coronary arteries. Int J Eng Sci 133:60–83

Gholipour A, Ghayesh MH, Zander A, Mahajan R (2018b) Three-dimensional biomechanics of coronary arteries. Int J Eng Sci 130:93–114

Kamali M, Mohamadhashemi V, Jalali A (2018) Parametric excitation analysis of a piezoelectric-nanotube conveying fluid under multi-physics field. Microsyst Technol 24:2871–2885. https://doi.org/10.1007/s00542-017-3670-8

Khaniki HB, Hosseini-Hashemi S, Khaniki HB (2018) Dynamic analysis of nano-beams embedded in a varying nonlinear elastic environment using Eringen's two-phase local/nonlocal model Eur Phys J Plus 133:283

Li L, Hu Y, Ling L (2016) Wave propagation in viscoelastic single-walled carbon nanotubes with surface effect under magnetic field

based on nonlocal strain gradient theory. Phys E Low Dimens Syst Nanostruct 75:118–124

Lim C, Zhang G, Reddy J (2015) A higher-order nonlocal elasticity and strain gradient theory and its applications in wave propagation. J Mech Phys Solids 78:298–313

Lin MX, Lai HY, Chen CK (2018) Analysis of nonlocal nonlinear behavior of graphene sheet circular nanoplate actuators subject to uniform hydrostatic pressure. Microsyst Technol 24:919–928. https://doi.org/10.1007/s00542-017-3406-9

Malekzadeh P (2007) A differential quadrature nonlinear free vibration analysis of laminated composite skew thin plates. Thin Walled Struct 45:237–250

Malekzadeh P, Shojaee M (2013a) Buckling analysis of quadrilateral laminated plates with carbon nanotubes reinforced composite layers. Thin Walled Struct 71:108–118

Malekzadeh P, Shojaee M (2013b) Surface and nonlocal effects on the nonlinear free vibration of non-uniform nanobeams. Compos Part B Eng 52:84–92

Malekzadeh P, Vosoughi A (2009) DQM large amplitude vibration of composite beams on nonlinear elastic foundations with restrained edges. Commun Nonlinear Sci Numer Simul 14:906–915

Malekzadeh P, Haghighi MG, Shojaee M (2014) Nonlinear free vibration of skew nanoplates with surface and small scale effects. Thin Walled Struct 78:48–56

Maraghi ZK, Arani AG, Kolahchi R, Amir S, Bagheri M (2013) Nonlocal vibration and instability of embedded DWBNNT conveying viscose fluid. Compos Part B Eng 45:423–432

Nejad MZ, Hadi A, Farajpour A (2017) Consistent couple-stress theory for free vibration analysis of Euler–Bernoulli nano-beams made of arbitrary bi-directional functionally graded materials. Struct Eng Mech 63:161–169

Paidoussis MP (1998) Fluid-structure interactions: slender structures and axial flow, vol 1. Academic Press, Cambridge

Pradiptya I, Ouakad HM (2018) Thermal effect on the dynamic behavior of nanobeam resonator assuming size-dependent higher-order strain gradient theory. Microsyst Technol 24:2585–2598. https://doi.org/10.1007/s00542-017-3671-7

Reddy J (2010) Nonlocal nonlinear formulations for bending of classical and shear deformation theories of beams and plates. Int J Eng Sci 48:1507–1518

Reddy J, Pang S (2008) Nonlocal continuum theories of beams for the analysis of carbon nanotubes. J Appl Phys 103:023511

Sahmani S, Aghdam MM (2018) Thermo-electro-radial coupling nonlinear instability of piezoelectric shear deformable nanoshells via nonlocal elasticity theory. Microsyst Technol 24:1333–1346. https://doi.org/10.1007/s00542-017-3512-8

Sassi SB, Najar F (2018) Strong nonlinear dynamics of MEMS and NEMS structures based on semi-analytical approaches. Commun Nonlinear Sci Numer Simul 61:1–21

Setoodeh A, Afrahim S (2014) Nonlinear dynamic analysis of FG micro-pipes conveying fluid based on strain gradient theory. Compos Struct 116:128–135

Soltani P, Taherian M, Farshidianfar A (2010) Vibration and instability of a viscous-fluid-conveying single-walled carbon nanotube embedded in a visco-elastic medium. J Phys D Appl Phys 43:425401

Wang Y-Z, Li F-M, Kishimoto K (2010) Wave propagation characteristics in fluid-conveying double-walled nanotubes with scale effects. Comput Mater Sci 48:413–418

Yayli MÖ (2018) Torsional vibrations of restrained nanotubes using modified couple stress theory. Microsyst Technol 24:3425–3435. https://doi.org/10.1007/s00542-018-3735-3

Zeighampour H, Beni YT (2014) Size-dependent vibration of fluid-conveying double-walled carbon nanotubes using couple stress shell theory. Phys E Low Dimens Syst Nanostruct 61:28–39

Zhang Y, Liu G, Xie X (2005) Free transverse vibrations of double-walled carbon nanotubes using a theory of nonlocal elasticity. Phys Rev B 71:195404

Zhu X, Li L (2017) Closed form solution for a nonlocal strain gradient rod in tension. Int J Eng Sci 119:16–28